Super-exponential growth and stochastic shape dynamics in rod-like bacteria

K. Callaghan Cylke[1] and Shiladitya Banerjee[1,*]

[1]*Department of Physics, Carnegie Mellon University, Pittsburgh, PA 15213, USA*

(Dated: May 21, 2022)

Proliferating bacterial cells exhibit stochastic growth and shape dynamics but the regulation of noise in bacterial growth and morphogenesis remains poorly understood. A quantitative understanding of morphogenetic noise control, and how it changes under different growth conditions, would provide better insights into cell-to-cell variability and intergenerational fluctuations in cell physiology. Using multigenerational growth and shape data of single *Escherichia coli* and *Caulobacter crescentus* cells, we deduce the equations governing growth and shape dynamics of bacterial cells. Interestingly, we find that both *E. coli* and *C. crescentus* cells grow faster than an exponential within a cell cycle, irrespective of nutrient or temperature conditions. We propose a mechanistic model that explains the emergence of super-exponential growth from autocatalytic production of ribosomes, coupled to the rate of cell elongation and surface area synthesis. Using this new model and statistical inference on large datasets, we construct the Langevin equations governing cell size and shape dynamics of *E. coli* cells in different growth conditions. The single-cell level model predicts how noise in intragenerational and intergenerational processes regulate variability in cell morphology and generation times, revealing quantitative strategies for cellular resource allocation and morphogenetic noise control in different growth conditions.

I. INTRODUCTION

Uncovering the quantitative principles of single-cell physiology demands high quality experimental data at the single-cell level with extensive statistics [1]. This information needs to be integrated with quantitative theory to interpret single-cell behaviors, inform the underlying mechanistic models, and direct new experimental research. Recent advances in single-cell imaging and microfluidics have resulted in large amounts of high-quality datasets on the size and shapes of single bacterial cells as they grow and divide [2–7]. These data have revealed many fundamental models and principles underlying single-cell physiology, including the mechanisms of cell size homeostasis and division control [4, 8–13], cell size control and growth physiology [12, 14–16], cell shape control [11, 17–19] and adaptation to environmental changes [20–23]. While extensive work has been done to characterize cell size regulation and division control at the inter-generational level [12], much less is understood about the dynamics of cell growth within an individual cell cycle. The bacterial cell cycle is composed of complex coupled processes, including DNA replication, cell wall synthesis and constriction, that have to be faithfully coordinated for cells to successfully divide. These processes require dynamic remodelling of the cell envelope and shape, raising questions on how cell growth and shape changes are dynamically coupled and how noise in these processes are regulated to ensure morphological stability through cycles of growth and division.

In this article, we develop quantitative theory for the stochastic growth and shape dynamics of rod-shaped bacterial cells using multigenerational growth and morphology data of *Escherichia coli* and *Caulobacter crescentus* cells [4, 11]. While there are existing studies using stochastic and deterministic models to describe bacterial growth and division processes [24–28], a common assumption in these models is that bacteria grow exponentially in cell size. Our analysis reveals that single *E. coli* and *C. crescentus* cells elongate faster than an exponential during the cell cycle, challenging existing models of exponential growth [2, 4, 5, 8, 9, 17, 24, 29]. We show that super-exponential growth naturally emerges in a model of autocatalytic production of ribosomes, which determine the speed of cell elongation and surface area synthesis. This model allows us to derive the equations governing the dynamics of cell length and width, showing that super-exponential elongation in cell length occurs non-uniformly along the cell, while cell width fluctuates around a mean value that is dependent on the growth rate. Analysis of noise in growth and shape parameters of *E. coli* cells [4] reveals strong intergenerational coupling of fluctuations in cell length and growth rate, whereas the fluctuations in cell width are independent of length. We then extend our dynamics into stochastic processes that accurately reflect the noise seen in experimental data as well as the correlations in model parameters across different growth conditions. In particular, we find that the dominant noise contributions come from model parameters that determine the rate of ribosomal synthesis, division protein synthesis, and cell surface area production. The resultant Langevin equations for cell length and width are capable of making predictions about the role of both intra-generational and inter-generational noise on the distribution of cell size and generation times in different nutrient conditions. Furthermore, using the single-cell level model we predict cellular strategies for ribosomal resource allocation and morphogenetic noise control in different growth conditions.

II. MODEL FOR CELL GROWTH

A common assumption in existing models of bacterial growth is that bacterial cells grow exponentially in size during the course of the cell cycle [2, 4, 5, 8, 9, 17, 24, 29]. We first re-examined this model by analyzing multi-genenerational growth and shape data of single *E. coli* cells grown in the mother machine under different nutrient conditions [4].

* shiladtb@andrew.cmu.edu

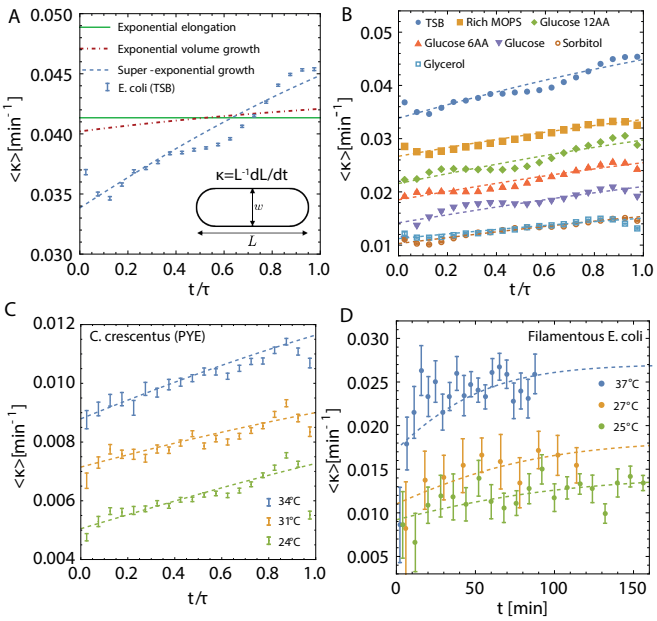

FIG. 1. **Super-exponential growth in *E. coli* and *C. crescentus* cells in different growth conditions.** (A) Ensemble-averaged instantaneous growth rate of *E. coli* cells grown in TSB media at $37°C$ vs normalized time t/τ, where τ is cell cycle duration. Data taken from [4]. Error bars in all parts show ± 1 standard error in the mean. The solid green line shows a fit of exponential length growth, dot-dashed blue represents a prediction from exponential volume growth (1), and dashed blue shows a fit to super-exponential growth (2). Inset: A simplified cell shape schematic for *E.* coli, defining the shape parameters. (B) Fits of super-exponential growth model (2) to average growth rate data for seven different growth conditions grown at $37°C$, taken from [4]. Error bars are negligible on the plotted scale. (C) Fits of super-exponential growth model (2) to average instantaneous growth rate vs t/τ of *C. crescentus* cells grown in PYE at three different temperatures. Data taken from [11]. (D) Time-dependent growth rate in filamentous *E. coli* cells grown in LB at different temperatures, presented in absolute time. Data taken from [6]. Dashed lines in (A-D) represent fits of the model in Eq. (2).

Parametrizing the geometry of rod-shaped *E. coli* cells by the pole-to-pole length L and width w (Fig. 1A-inset), we define the instantaneous growth rate as $\kappa(t) = L^{-1}\mathrm{d}L/\mathrm{d}t$. To determine the overall trend in growth rate during the cell cycle, we averaged growth rate data across individual generations to obtain the average growth rate $\langle\kappa\rangle$ vs t/τ, where t is the time since birth and τ is the interdivision time. We found that the growth rate of the cell increases by $\sim$30% during the cell cycle in fast growth conditions (Fig. 1A), consistent with recent reports of increase in *E. coli* growth rate during the cell cycle [6, 30]. This trend in super-exponential growth is preserved across different nutrient conditions (Fig. 1B), thereby invalidating existing models of purely exponential growth. As a test of whether this behavior is specific to *E. coli*, we applied the same analysis to rod-shaped *C. crescentus* cells grown in nutrient-rich media (PYE) at different temperatures [5, 11]. Our analysis confirms that *C. crescentus* cells elongate faster than exponential (Fig. 1C), suggesting that super-exponential growth is likely prevalent across different bacterial species.

To understand the mechanistic origin of super-exponential growth, we first inquired if the increase in the rate of elongation in cell length is a geometric consequence of exponential growth in cell volume V [17, 31], $\mathrm{d}V/\mathrm{d}t = k_V V$, where k_V is the constant rate of volume growth. Assuming a spherocylinderical cell geometry, we derive the length equation

$$\frac{\mathrm{d}L}{\mathrm{d}t} = k_V\,(L - w/3)\ , \tag{1}$$

which can be interpreted as exponential growth of a portion $L - w/3$ of the cell's total length. As seen in Fig. 1A, this model leads to a $\sim$3% increase in κ over time, which is an order of magnitude less than what is observed in the data.

Recent experiments have shown that the *E. coli* and *C. crescentus* cells do not grow uniformly along their length [11, 32], motivating a physical model where a portion λ of the total cell length does not grow:

$$\frac{\mathrm{d}L}{\mathrm{d}t} = k(L - \lambda)\ , \tag{2}$$

where k is the rate of cell elongation and the parameter λ can be determined by fitting the model to experimental data. This phenomenological model makes no assumptions about the spatial distribution of λ, but assumes that λ is time-independent. Attempts to model time-dependent λ results in inconsistencies with experimental data for *E. coli* or *C. crescentus*; increasing λ over time leads to sub-exponential growth, whereas a decrease in λ results in unbounded increase in growth rate that is inconsistent with data for filamentous cells (see below). Solving Eq. (2) for $0 \le t \le \tau$ gives

$$L(t) = \lambda + (L_0 - \lambda)e^{kt}, \tag{3}$$

where L_0 is the cell length at birth. Since *E. coli* behaves as an adder [4, 8, 9], cell division occurs when the cell length increments by a constant amount Δ: $L(\tau) = L_0 + \Delta$. Thus the interdivision time is given by $\tau = k^{-1}\ln\left(1 + \Delta/(L_0 - \lambda)\right)$. Upon division, each daughter cell is assigned a value of λ uncorrelated to that of the mother cell (Table II).

Comparison between the models given by Eq. (1) and (2) are provided in the data for cell length vs time (Supplementary Fig 1A-B) and growth rate vs time (Fig. 1A-B). For the length data, goodness of fit tests reveal that model (2) most accurately captures the data (Supplementary Fig 1C). With the model parameters determined from fitting the cell length data, model (2) is capable of fully capturing the increasing growth rate trend (Fig. 1A) across all nutrient conditions (Fig. 1B). Interestingly, we find that the average value of λ is larger than the average cell diameter in all growth conditions (Fig. 2B), suggesting that there are regions within the cylindrical portion that are non-growing in addition to the poles.

A key prediction of our model is that the growth rate of the cell saturates to a constant at longer times, such that cell growth becomes purely exponential. This is evident from the growth rate equation

$$\frac{\mathrm{d}\kappa}{\mathrm{d}t} = -\kappa(\kappa - k)\ , \tag{4}$$

which predicts that $\kappa \approx k$ for $t \gg \kappa^{-1}$. To test this prediction, we analyzed the morphologies of filamentous *E. coli* cells [6] that have longer cell cycles due to impaired division. In agreement with our model, data show that the growth rate of filamentous cells increases initially and then saturates to a constant value over longer times ($\sim$ 100 min at 25°C and 27°C), as shown in Fig. 1D. The timescale to reach exponential growth phase decreases with temperature, and thereby decreases with increasing growth rate, which is in agreement with our theory.

Our phenomenological model of super-exponential growth can be derived from an underlying molecular model that assumes cell length increases at a rate proportional to the abundance R of actively translating ribosomes

$$\frac{\mathrm{d}L}{\mathrm{d}t} = \alpha R \ , \tag{5}$$

where α is the speed of cell elongation per ribosome, related to the translational capacity of the cell. This model is motivated by data that bacterial growth rate is linearly proportional to the mass fraction of actively translating ribosomes [33]. Since ribosomes are autocatalytic structures, the abundance of active ribosomes grows at a rate proportional to R

$$\frac{\mathrm{d}R}{\mathrm{d}t} = kR \ , \tag{6}$$

where k defines the rate of synthesis of ribosomal proteins. Solving for $L(t)$, we arrive at the same equation as (3) with

$$\lambda = L_0 - \alpha R_0/k \ , \tag{7}$$

where R_0 is the abundance of active ribosomes at cell birth, k is identified as the cell elongation rate (3), predicting that λ increases with k. In this form, λ is more clearly interpreted as the difference between cell's actual length (L_0) and the amount of length material synthesized by ribosomes ($\alpha R_0/k$) at birth. Thus, super-exponential growth arises when there is a mismatch between cell geometry and the initial protein synthesis capacity of the cell. Furthermore, cell growth is coupled to division such that the production rate of division proteins X (e.g., FtsZ) is proportional to the amount of active ribosomes [34, 35],

$$\frac{\mathrm{d}X}{\mathrm{d}t} = \beta R \ , \tag{8}$$

where X is the division protein abundance and β is the rate of synthesis of division proteins per ribosome. Cells divide once a threshold amount of division proteins, X_0, are synthesized during the cell cycle [13, 22, 34, 35]. This leads to an adder model for cell size control, such that the added cell length (Δ) during each division cycle is given by

$$\Delta = X_0 k^2/(\alpha\beta). \tag{9}$$

An adder mechanism for cell length control implies an adder model for ribosome homeostasis, such that $R_n(\tau) = R_{0,n} + k\Delta_n/\alpha$, where n is the generation index. Following division, $R_{0,n+1} = \frac{1}{2}R_n(\tau) - R^{\mathrm{U}}_{n+1}$, where R^{U}_{n+1} is the amount of ribosomes unused for cell growth (or degraded) in generation $n+1$. A non-zero R^{U} is necessary for continuing super-exponential growth in consecutive generations, as observed in data (Supplementary Fig 1D), otherwise a cell would quickly attain exponential growth following division (see Supplementary Information for details).

III. INTERGENERATIONAL FLUCTUATIONS IN CELLULAR GROWTH PARAMETERS

While the deterministic growth model described by Eqs. (5)-(6) accurately describes the average growth dynamics of the cell, there are significant fluctuations in model parameters across different generations and growth conditions. Understanding these parameter variations is essential for predictive modeling of stochastic growth dynamics. To obtain a quantitative understanding of the noise in the cellular growth parameters between individual generations, we move from fitting ensemble-averaged data to individual generations within each growth condition for *E. coli* (Supplementary Fig 1A) [4]. Fitting our effective growth model (2) to cell length data for each generation provides a pair of values for the elongation rate, k, and the effective length of the non-growing region, λ. From these fits, we find a positive correlation between k and λ within each growth condition, as shown by the scatterplot in Fig 2A. The mean trend in the correlation between λ and k is accurately captured by Eq. (7), which predicts that λ increases with k. Furthermore, we observe a strong positive correlation between the population means $\langle\lambda\rangle$ and $\langle k\rangle$ across nutrient conditions (Fig. 2B). To understand the origin of this correlation, we compute the relationship between $\langle\lambda\rangle$ and $\langle k\rangle$ using (7) under a small-fluctuation approximation in k,

$$\langle\lambda\rangle \approx \langle L_0\rangle - \langle\alpha R_0\rangle(\langle k\rangle^{-1} + \sigma_k^2\langle k\rangle^{-3}) \ , \tag{10}$$

where σ_k is the standard deviation in k. In the above equation, both $\langle L_0\rangle$ and $\langle\alpha R_0\rangle$ are functions of $\langle k\rangle$. Since average cell size increases exponentially with the nutrient-specific growth rate [14, 36], we assume an exponential form for the dependence of $\langle L_0\rangle$ on $\langle k\rangle$ that we determine by fitting experimental data [4] (Supplementary Fig 2A). Furthermore, since ribosome mass fraction increases linearly with growth rate [33], we fit $\langle\alpha R_0\rangle/\langle L_0\rangle$ to a linear function of $\langle k\rangle$ that captures the data very well (Supplementary Fig 2B). With these fitted functions, we can model $\langle\lambda\rangle$ as a continuous function of $\langle k\rangle$ (Fig. 2B).

Next we turn to modeling the distributions of λ and k such that the intergenerational correlations are accurately captured. Marginalizing the joint distribution of k and λ obtained from experimental data, we find that the probability distributions of $\delta k = k - \langle k\rangle$ and $\delta\lambda = \lambda - \langle\lambda\rangle$ are skewed right and left, respectively, with increasing variance as $\langle k\rangle$ increases (Fig. 2C-D). We observe that the variations in k are reasonably well approximated by a log-normal distribution, as shown in Fig. 2D. This is not unexpected as the cellular elongation rate k is an accumulation of growth at many individual sites on the

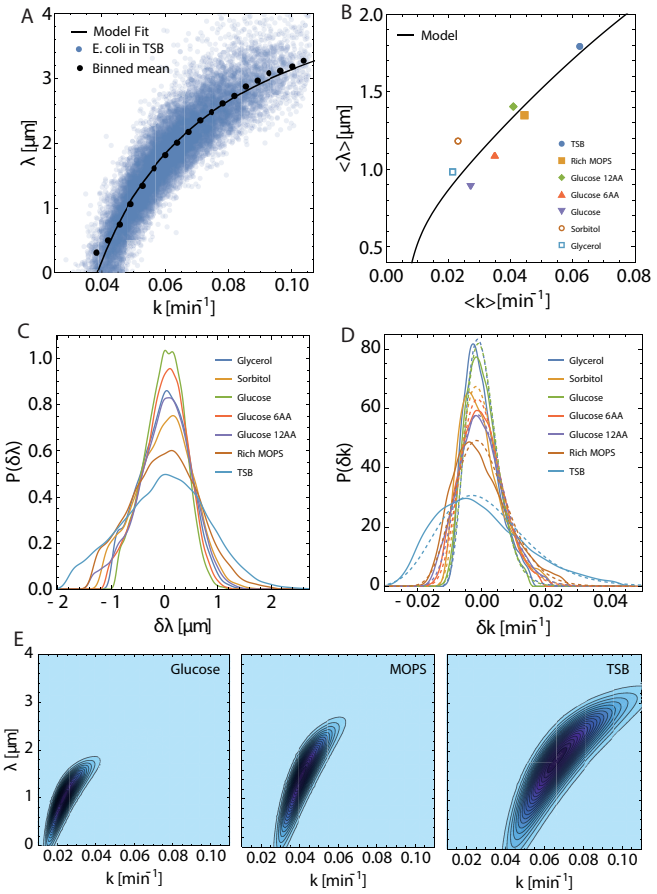

FIG. 2. **Intergenerational fluctuations and correlations in *E. coli* cell growth parameters.** (A) Scatterplot showing the correlation between k and λ obtained by fitting super-exponential growth model to *E. coli* cell length vs time data in TSB. The solid black curve represents a fit of Eq. (7) to the data. We remove outliers and the small number of generations in fast growth conditions with $\lambda < 0$ from further analysis (see Methods). (B) Ensemble-averaged $\langle\lambda\rangle$ vs $\langle k\rangle$ across different growth conditions. The black curve is a model prediction for $\langle\lambda\rangle$ as a function of $\langle k\rangle$ according to Eq. (10), with $\langle L_0\rangle = (1.50\ \mu m)\exp((16.19\ \text{min})\langle k\rangle)$, $\langle\alpha R_0\rangle = (0.84\ \mu m)\langle k\rangle\exp((16.19\ \text{min})\langle k\rangle)$, $\sigma_k^2 = (11.14\ \text{min}^2)\langle k\rangle^4 + (2.67\cdot 10^{-5})\ \text{min}^{-2}$. (C) Marginal probability distributions of $\delta\lambda = \lambda - \langle\lambda\rangle$ across different growth conditions. (D) Marginal probability distributions of $\delta k = k - \langle k\rangle$ for each growth condition shown as solid color curves. Dashed curves of the same color depict fits of log-normal distributions. Experimental data presented in (A-D) are taken from [4]. (E) Representative contour plots of the model predictions for the joint distribution $P(k,\lambda)$, corresponding to mean growth rates in Glucose, MOPS, and TSB media. Darker blue indicates higher probability.

surface of the cell. However, the distribution of λ is slightly more difficult to model analytically (Fig. 2C). The unusual shape for λ distribution arises from the noise in L_0, k, α and R, through the relation defined in Eq. (7). Even under Gaussian noise approximations, an exact analytical distribution for λ does not exist. However, assuming small fluctuations about

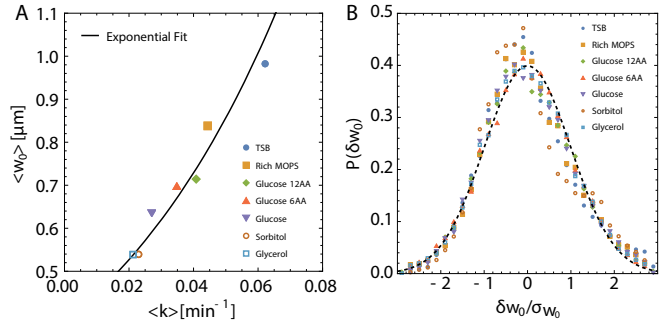

FIG. 3. **Intergenerational variations in *E. coli* cell width across growth conditions.** (A) Average width $\langle w_0\rangle$ vs $\langle k\rangle$ across growth conditions. The solid black line shows that $\langle w_0\rangle$ increases exponentially with $\langle k\rangle$, keeping a fixed length-width aspect ratio ($\langle w_0\rangle = 0.25\langle L_0\rangle = (0.38\ \mu m)\exp((16.19\ \text{min})\langle k\rangle)$). (B) Probability distributions of the intergenerational fluctuations $\delta w_0 = w_0 - \langle w_0\rangle$ across growth conditions scaled by their respective standard deviations ($\sigma_{w_0} = 0.06\langle w_0\rangle = (0.02\ \mu m)\exp((16.19\ \text{min})\langle k\rangle)$). The dashed curve shows a universal Gaussian fit to the scaled data. Data are taken from [4].

the mean values, we find that

$$\sigma_\lambda \approx \sqrt{\sigma_{L_0}^2 + \frac{\langle\alpha R_0\rangle^2\sigma_k^2 + \langle k\rangle^2\sigma_{\alpha R_0}^2}{\langle k\rangle^4}}\ , \qquad (11)$$

where σ_i is the standard deviation in parameter i. Interestingly, larger values of $\langle\alpha R_0\rangle$ leads to greater contribution of the noise in k, whereas larger $\langle k\rangle$ increases the contribution of the noise in αR_0. An approximate analytical form the joint distribution $P(k,\lambda)$ can be constructed by transforming the variables k and λ to remove the skew in the distribution: $K = \ln k$ and $\Lambda = \sqrt{\lambda_0 - \lambda}$, where λ_0 is a chosen reference value. The transformed variables K and Λ are normally distributed, allowing us to construct a correlated multivariate normal distribution, $P(K,\Lambda)$ (see Methods), whose parameters can be fitted with appropriate mathematical functions of the average elongation rate $\langle k\rangle$ (Supplementary Fig 3). Representative contour plots of the joint distribution P are shown in Fig. 2E for three different growth conditions.

IV. CELL SHAPE MAINTENANCE DURING GROWTH

While cell length increases during the cell cycle, the width of rod-shaped *E. coli* fluctuates about a mean value w_0 [4]. We consider two levels to these fluctuations: fluctuations of cell mean width w_0 about the population mean $\langle w_0\rangle$, and temporal fluctuations in cell width w about its mean w_0 during any given generation. Fig. 3 characterizes the statistical properties of w_0 as a function of the elongation rate k. Not surprisingly, $\langle w_0\rangle$ increases exponentially with $\langle k\rangle$ at the same rate as cell length (Fig. 3A). This is a consequence of *E. coli* cells maintaining a constant aspect ratio (on average) in different nutrient conditions [19]. The distribution of w_0 can be reasonably well approximated by a Gaussian, with the standard devia-

tion of w_0 increasing with $\langle k \rangle$ (Supplementary Fig 4A). In addition, the coefficient of variation in w_0 is roughly constant with changing growth conditions (Supplementary Fig 4B). As a result, the probability distribution of $\delta w_0/\langle w_0 \rangle$, where $\delta w_0 = w_0 - \langle w_0 \rangle$, can be collapsed onto a single Gaussian distribution (Fig. 3B).

To arrive at a general equation that describes the maintenance of cell width and its fluctuations around a mean value, we begin with the model that the surface area S of the cell is synthesized at a rate proportional to ribosomal abundance R,

$$\frac{\mathrm{d}S}{\mathrm{d}t} = \gamma R \,, \tag{12}$$

where γ is the rate of synthesis of surface material. This model stands in contrast to a recently proposed model of surface area synthesis in proportion to cell volume [17], but conceptually similar since surface material is assumed to be produced in the cytoplasm. Using a spherocylindrical geometry of the cell with pole-to-pole length L and width w, we have $S = \pi w L$. Using $\mathrm{d}L/\mathrm{d}t = \alpha R$ together with Eq. (12), we arrive at the width equation

$$\frac{\mathrm{d}w}{\mathrm{d}t} = \frac{\alpha R}{L}(w_0 - w) \,, \tag{13}$$

with $w_0 = \gamma/\pi\alpha$. Thus, w relaxes to the value w_0 at steady-state, with R/L approaching the value k/α. Since the coefficient of variation in w_0 is roughly constant across growth conditions (Fig 3B), it is reasonable to assume that the coefficients of variation in parameters α and γ are also maintained constant across different growth conditions.

Expressing R in terms of L and λ yields an alternative form for the width equation

$$\frac{\mathrm{d}w}{\mathrm{d}t} = k\left(1 - \frac{\lambda}{L}\right)(w_0 - w) \,, \tag{14}$$

which showcases the asymptotic approach to $\mathrm{d}w/\mathrm{d}t \approx k(w_0 - w)$, without considering the dynamics of R directly. This approach occurs on the timescale of the generation time τ, taking around 3τ to stabilize (Supplementary Fig 4C). Taken together, Eq. (2) and (14) describe the intra-generational shape dynamics of a bacterial cell, characterized by only three parameters, k, λ, and w_0, which vary across generations and growth conditions. Next, we turn to computing the intergenerational correlations in these parameters, in order construct a stochastic model for cell shape dynamics as it evolves through cycles of birth, growth and replication.

V. CORRELATIONS IN MODEL PARAMETERS

There are two levels at which we must address the correlations in our model parameters: correlation between mother and daughter cells and population-wide correlation. In Table I, we list the intergenerational correlations in model parameters for each growth condition. As shown earlier in Fig. 2A, there is a strong positive correlation between λ and k. However, we do not observe a correlation between either k or λ with w_0. This simplifies our model immensely since the length and width equations can now be simulated independently. It is interesting to note that there is a slight positive correlation between λ and the initial cell length L_0, which decreases with increasing $\langle k \rangle$. This makes intuitive sense since λ is a portion of L_0, and as L_0 increases with growth rate the possible values of λ are less constrained. In other words, the contribution of αR_0 in (7) is more pronounced for faster growing cells. We do not observe any substantial correlations between the added size Δ and the growth parameters k and λ.

TABLE I. Intergenerational correlations of model parameters

Growth Condition	$\rho(k,\lambda)$	$\rho(\lambda,w_0)$	$\rho(k,w_0)$	$\rho(\lambda,L_0)$
Glycerol	0.86	-0.07	-0.05	0.26
Sorbitol	0.84	-0.09	0.04	0.20
Glucose	0.88	-0.07	0.01	0.21
Glucose 6AA	0.89	0.02	0.12	0.21
Glucose 12AA	0.92	-0.02	0.09	0.14
Rich MOPS	0.87	-0.07	0.05	0.07
TSB	0.89	-0.16	-0.03	0.10

TABLE II. Correlations between successive generations

Growth Cond.	$\rho_{n,n+1}(k)$	$\rho_{n,n+1}(\lambda)$	$\rho_{n,n+1}(L_0)$	$\rho_{n,n+1}(w_0)$
Glycerol	0.03	0.05	0.54	0.77
Sorbitol	0.00	-0.01	0.56	0.59
Glucose	0.01	0.04	0.55	0.75
Glucose 6AA	0.00	0.03	0.51	0.81
Glucose 12AA	0.00	0.05	0.52	0.78
Rich MOPS	0.00	0.01	0.48	0.72
TSB	0.00	0.07	0.50	0.82

In Table II we examine the correlations in model parameters between successive generations. As expected from the adder model [12], there is a positive correlation in subsequent values of L_0, with a correlation coefficient ≈ 0.5. Despite the slight positive correlation between L_0 and λ at the population level (Table I), we see no correlation in λ values between successive generations. Furthermore, there is no correlation between subsequent generation values of k, so both k and λ can be drawn independently for each generation from the joint distribution $P(k,\lambda)$ (Eq. 25). However, cell mean width is highly correlated between the mother and the daughter cell, such that the mean width in successive generations are related as

$$w_{0_{n+1}} = \sigma_{w_0}\left(\rho\,\frac{w_{0_n} - \langle w_0 \rangle}{\sigma_{w_0}} + \mathcal{N}\right) + \langle w_0 \rangle \,, \tag{15}$$

where ρ is the correlation between $w_{0_{n+1}}$ and w_{0_n}, and $\mathcal{N}$ is a Gaussian with mean 0 and variance $1-\rho^2$. With all the intergenerational correlations accounted for, we now turn to developing the Langevin equations for cell length and width that can accurately capture intra-generational correlations and

fluctuations in cell morphology and growth rates.

VI. STOCHASTIC GROWTH AND SHAPE DYNAMICS

To simulate the stochastic growth and shape dynamics of single cells, we account for the noise in model parameters within each generation. We derive the Langevin equations governing the dynamics of cell length and width by considering noise in the parameters defining the deterministic equations (5)-(6), and (12). To this end, we write each parameter q ($\alpha, k,$ or γ) as $q(t) = \bar{q} + \nu_q(t)$, where $\bar{q}$ represents the average value of the parameter within a generation and $\nu_q(t)$ represents the time-dependent intra-generational fluctuations in q, assumed to be Gaussian white noises with zero mean. Considering stochastic variations in the parameters α and γ, we write the equation for cell width (13) as

$$\frac{\mathrm{d}w}{\mathrm{d}t} = \bar{\alpha}\frac{R}{L}\left(w_0 - w\right) + \frac{R}{L}\left(\frac{\nu_\gamma}{\pi} - w\nu_\alpha\right), \qquad (16)$$

where $w_0 = \bar{\gamma}/\pi\bar{\alpha}$. Considering the deviations from the cell mean width $\delta w = w - w_0$, we find

$$\frac{\mathrm{d}\delta w}{\mathrm{d}t} = -\bar{\alpha}\frac{R}{L}\delta w + \frac{R}{L}\underbrace{\left(\frac{\nu_\gamma}{\pi} - w_0\nu_\alpha\right)}_{\eta_w} + \frac{R}{L}\nu_\alpha\delta w\ , \qquad (17)$$

where η_w is a time-uncorrelated Gaussian additive noise with amplitude $\sigma^2_{\eta_w}$, $\langle\eta_w(t)\eta_w(t')\rangle = \sigma^2_{\eta_w}\delta(t-t')$. In addition, fluctuations in α, characterized by the noise ν_α, contributes to multiplicative noise in the width equation. The interplay between additive and multiplicative noise with a restorative drift has been studied recently in the context of bacterial shape control [27]. Although our equation differs from [27], some of the conceptual results in [27] hold here as well. Crucially, the effect of increased multiplicative noise on the distribution of δw is to not only increase the spread but also to add a positive skew to the distribution. In other words, neglecting the multiplicative noise ($\nu_\alpha = 0$) to write

$$\frac{\mathrm{d}\delta w}{\mathrm{d}t} = -\bar{\alpha}\frac{R}{L}\delta w + \frac{R}{L}\eta_w \qquad (18)$$

is a good approximation when δw is Gaussian. As a result, δw follows an Ornstein-Uhlenbeck process [37]. From the experimental data, we do not observe a skew to δw distribution and hence this approximation is justified. Neglecting the multiplicative noise is equivalent to neglecting intra-generational variations in α compared to k and γ.

Integrating Eq. (17) would require keeping track of the values of R as it fluctuates during growth. While this mathematically poses no difficulty, we do not currently have experimental data for the dynamics of $R(t)$, so their values cannot be benchmarked in simulations. To circumvent this issue, we eliminate R to recast the width equation in terms of L:

$$\frac{\mathrm{d}\delta w}{\mathrm{d}t} = -\bar{k}\left(1 - \frac{\lambda}{L}\right)\delta w + \left(1 - \frac{\lambda}{L}\right)\eta_w\ , \qquad (19)$$

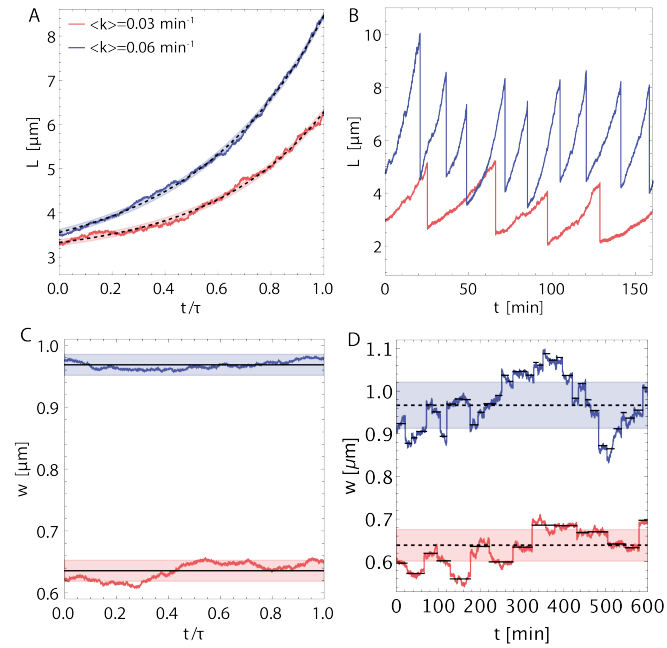

FIG. 4. **Langevin simulations for stochastic cell shape dynamics in fast and slow growth conditions.** For (A-D), blue trajectories correspond to a relatively fast growing condition with $\langle k\rangle = 0.06\ \mathrm{min}^{-1}$ and red to a relatively slow growing condition with $\langle k\rangle = 0.03\ \mathrm{min}^{-1}$. (A) Length vs normalized time t/τ for a single generation, where τ is cell cycle duration. The dashed black curve is a fit of deterministic super-exponential growth (2). The transparent bands surrounding each deterministic curve represent the standard deviation in length fluctuations ($\sigma_{\delta L} = 0.066\ \mu m$). (B) Length vs absolute time for several generations. (C) Width vs t/τ for a single generation in normalized time. The solid black shows individual cell mean width. The transparent band around each cell mean width line represents the standard deviation in width fluctuations ($\sigma_{\delta w} = 0.017\ \mu m$). (D) Width vs absolute time for several generations. Cell mean width is represented with solid black lines while population mean width is represented by dashed black. The transparent band around each population mean width line represents the standard deviation in intergenerational fluctuations ($\sigma_{w_0} = (0.02\ \mu m)\exp((16.19\ \mathrm{min})\langle k\rangle)$).

which can be integrated forward using information available from data. In the case of purely exponential growth in length ($\lambda = 0$), (19) takes the simple form

$$\frac{\mathrm{d}\delta w}{\mathrm{d}t} = -\bar{k}\delta w + \eta_w\ , \qquad (20)$$

showing that width fluctuations decay over a timescale $\bar{k}^{-1}$ that is set by the elongation rate. Since $(1 - \lambda/L)$ scales both the restoring force and the noise in the width equation, despite $(1-\lambda/L)$ increasing throughout the cell cycle we see no qualitative or quantitative differences between width trajectories generated by model (19) or (20) (Supplementary Fig 5). In other words, super-exponential elongation in length does not strongly affect stochastic width fluctuations within a generation. The langevin equation for cell length can be derived

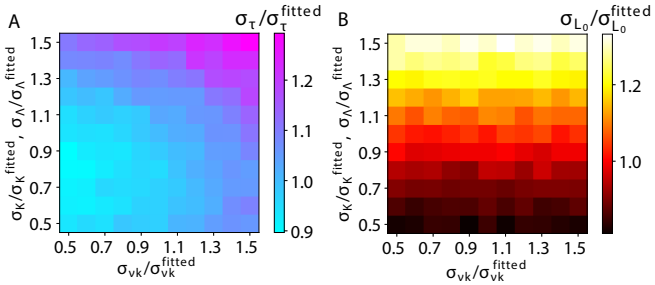

FIG. 5. **Noise in cell cycle time and cell size propagates from noise in growth parameters.** (A) A colormap showing standard deviation in cell cycle time τ (σ_τ) predicted by our stochastic simulations, as a function of intergenerational noise (σ_K, σ_Λ) and intra-generational noise ($\sigma_{\nu k}$). Each axis is normalized by dividing the varied parameter(s) by the standard value(s) fitted to the data, and the scale of σ_τ is likewise normalized by the unperturbed value. Each parameter is varied $\pm 50\%$ along each axis. Bins sample 5000 generations for a single cell. (B) A colormap showing normalized standard deviation in initial cell size ($\sigma_{L_0}/\sigma_{L_0}^{\text{fitted}}$), predicted by our simulations, as a function of intergenerational and intra-generational noise.

using Eq. (5),

$$\frac{\mathrm{d}L}{\mathrm{d}t} = \bar{\alpha}R + R\nu_\alpha \ . \tag{21}$$

By eliminating R and neglecting the intra-generational noise in α (as justified earlier) we can recast the above equation in terms of $\ell = L - \lambda$:

$$\frac{\mathrm{d}\ell}{\mathrm{d}t} = \bar{k}\ell + \ell\nu_k \ , \tag{22}$$

with multiplicative Gaussian white noise ν_k, where $\langle \nu_k \rangle = 0$, $\langle \nu_k(t)\nu_k(t') \rangle = \sigma^2_{\nu_k}\delta(t-t')$, and $\sigma^2_{\nu_k}$ is the noise amplitude. The above equation may be recognized as the Black-Scholes model in stochastic form [37]. As for stochastic variations in λ within a generation, it follows from Eq. (7) that

$$\lambda = L_0 - \frac{\alpha R_0}{k} \approx L_0 - \frac{\bar{\alpha}R_0}{\bar{k}+\nu_k} \approx L_0 - \frac{\bar{\alpha}R_0}{\bar{k}}\left(1 - \frac{\nu_k}{\bar{k}}\right), \tag{23}$$

which is approximately constant in the small fluctuation limit $\nu_k \ll \bar{k}$. This is implicit in the assumption of writing the noise term ν_k in Eq. (22). Rather than modeling k stochastically and updating L deterministically from k, we consider the fluctuations in k to be Gaussian around a mean $\bar{k}$, with no memory at each timestep during the cell cycle. While we don't model R directly to predict length and width dynamics, its dynamics can be derived by considering noise in k,

$$\frac{\mathrm{d}R}{\mathrm{d}t} = \bar{k}R + R\nu_k \ . \tag{24}$$

In other words, we predict a multiplicative noise in R with an amplitude $\sigma^2_{\nu_k}$ that can be determined from the measurements of length fluctuations.

With all the model parameters and their intra-generational and intergenerational fluctuations determined from experimental data, we can simulate the Langevin equations (19) and (22) in different growth conditions (see Methods). Fig. 4 shows representative trajectories of cell length and width resulting from such a simulation in fast and slow growth conditions. For both length and width, the simulations reproduce short timescale fluctuations within a given generation (4A and 4C), as seen in experimental data [4]. Longer timescale intra-generational length fluctuations about a smooth fit of (3) are also present, often spending $\sim$ 10-20% of the cell cycle above or below the average dynamics. The fluctuations about the intra-generational width mean are more pronounced than what we see for length dynamics, often spending more than $\sim 50\%$ of a cell cycle without crossing the mean, consistent with experimental data [4]. At the intergenerational level, length fluctuations are regulated by the adder model (4B) but the fluctuations in width dynamics (4D) are worth noting. Based on our observed mother-daughter correlations in w_0 (Table II), there is typically a large change in w during the division process compared to the intra-generational fluctuations.

The Langevin model can be used to generate predictions about the distribution of cell size and interdivision time. In Fig. 5, we simulate how the noise in cell cycle time (A) and initial cell size (B) changes as a function of the noise in growth at the intra- and intergenerational levels. Noise in added length Δ is propagated through from k according to Eq. (9). We observe that, while both intergenerational noise (σ_k, σ_λ) and intra-generational ($\sigma_{\nu k}$) noise have an impact on the fluctuations in generation time, the effects of the intergenerational noise are more pronounced. Assuming symmetric division, cell size distribution at birth is controlled entirely by Δ and, while Δ does fluctuate in time with ν_k, the time-uncorrelated fluctuations in $\bar{k}$ are too small to have an effect comparable to the cell-to-cell variation in Δ.

VII. SINGLE-CELL LEVEL RESOURCE ALLOCATION AND NOISE CONTROL STRATEGIES

The kinetic model we developed for stochastic cell growth and shape control can be used to derive single-cell level strategies for ribosomal resource allocation and morphogenetic noise control in different nutrient conditions. Previous studies on bacterial growth physiology at the population-level have revealed how bacteria allocate resources between ribosomal and metabolic protein synthesis in different nutrient conditions and under antibiotic treatments [33]. In particular, it was shown that there is a tradeoff between the mass fractions of ribosomal and metabolic proteins as nutrient conditions are varied [33]. Here we ask how such nutrient-dependent tradeoffs arise at the single-cell level between the allocation of cellular resources for growth, division and cell shape maintenance. Furthermore, we inquire how cells regulate noise in different physiological parameters as nutrient conditions are varied. Fig. 6A summarizes the main components of our model as defined by Eqs. (5)-(6), (8), and (12). Specifically, ribosomal proteins are involved in four major tasks: (1) production of ribosomes at a rate k, (2) cell elongation at a rate α, (3) division protein synthesis at a rate β, and (4) surface area synthesis at

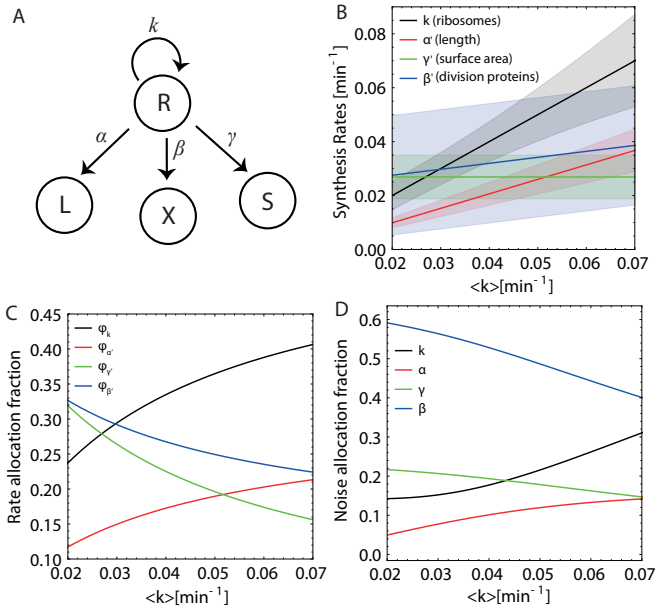

FIG. 6. **Cellular resource allocation and noise control strategies across nutrient conditions.** (A) A network diagram for the underlying protein synthesis model. Ribosomes (R) responsible for synthesising new proteins do so in an auto-catalytic process (rate k) while also producing proteins necessary for growth and division (rates α, β, and γ). (B) Normalized synthesis rates ($\alpha' = \alpha R_0/L_0$, $\gamma' = \gamma R_0/S_0$, $\beta' = \beta/(R_0 X_0)$) as a function of the mean elongation rate $\langle k \rangle$. Solid lines depict the mean values of the normalized rates, determined from fitting our model to data, and the transparent bands show one standard deviation of the corresponding distributions (see Methods). (C) Mean rates (as depicted in (B)) normalized by the sum of all rates for a given $\langle k \rangle$. (D) The noise (standard deviation) in each rate corresponding to the transparent bands in (B) normalized by the sum of all rates at a given $\langle k \rangle$.

a rate γ. All these rates are controlled by the nutrient-specific growth rate. While we can determine k by directly fitting cell length data, we cannot directly extract the absolute values of the rates α, β, and γ from data. We therefore define normalized synthesis rates (same physical units as k): $\alpha' = \alpha R_0/L_0$, $\gamma' = \gamma R_0/S_0$, $\beta' = \beta/(R_0 X_0)$, which can be determined from fitting *E. coli* cell length and width data [4] considered in prior sections.

From fits of our model to experimental data, we find that both $\langle \alpha' \rangle$ and $\langle \beta' \rangle$ increase with $\langle k \rangle$ while $\langle \gamma' \rangle$ remains approximately constant (Fig. 6B). At the resolution of the data and our fitting, we see no change in the amplitude of noise in γ' and β', while the noise in α' and k increases with $\langle k \rangle$. The increase in the rate of production of length material ($\langle \alpha' \rangle$) and the rate of division protein synthesis ($\langle \beta' \rangle$) with $\langle k \rangle$ is consistent with data that both cell size and the rate of cell division increase with growth rates [13, 14, 34]. Since the rate of production of surface material remains approximately constant with increasing growth rate and cell size, it implies that surface-to-volume ratio decreases with growth rate, as seen in experimental data [14, 17, 19].

Given that most of the synthesis rates increase with $\langle k \rangle$, it is more insightful to interpret these results in the context of allocation of ribosomal resources to each these physiological tasks. We therefore introduce the rate allocation fractions, ϕ_q ($q \in \{k, \alpha', \beta', \gamma'\}$), defined as the mean value of the rates $\langle q \rangle$, normalized by the sum of all mean rates ($\sum \langle q \rangle = \langle k + \alpha' + \beta' + \gamma' \rangle$). As shown in Fig. 6C, both ϕ_k and $\phi_{\alpha'}$ increases as $\langle k \rangle$ increases, while $\phi_{\beta'}$ and $\phi_{\gamma'}$ decreases with $\langle k \rangle$. It thus becomes clear that as nutrient-specific growth rates increase, cells allocate more ribosomal resources to producing more ribosomes and increasing cell size (length), while proportionally less resources are allocated to the production of cell division proteins and surface area synthesis. This trend can also be seen in noise allocation fractions reported in Fig. 6D, where we find that the relative noise in k and α' increases while those of γ' and β' decreases with increasing $\langle k \rangle$. Taken together, these data show that there is a nutrient-dependent tradeoff between cellular resources allocated ribosome synthesis and cell size, and those that are allocated to synthesizing cell surface area and division proteins. These tradeoffs underlie the control of bacterial cell growth and morphology, and the regulation of noise in cellular growth and morphogenetic parameters.

VIII. DISCUSSION

The predominant assumption for most of the history of bacterial growth modeling has been that exponential growth occurs at both the population and individual scales [12]. Our observations contradict this standard; we find super-exponential growth in cell length and volume for rod-shaped bacteria across a variety of nutrient and temperature conditions. We propose mechanistic models that account for the increasing growth rate during the cell cycle – first in terms a phenomenological model of non-uniform exponential growth, and second in terms of a biochemical model of autocatalytic ribosome synthesis. In the phenomenological model of non-uniform growth, the non-growing region of the bacterial cell can be interpreted using the biochemical model as the mismatch between the cell's geometry and initial capacity to synthesize proteins necessary for growth. All of the parameter distributions that make up the dynamic models for cell growth, division, and width maintenance have been parametrized as functions of cellular elongation rate alone, allowing us to make quantitative predictions for how the average values and the noise in cellular parameters evolve in arbitrary growth conditions. Combining intergenerational noise factors with intragenerational stochastic differential equations, we uncover the degrees to which various underlying noise sources in growth and division processes contribute to overall noise in bacterial growth and morphogenesis.

While our stochastic growth model is developed primarily using single-cell data for *E. coli*, the modeling approach could be extended to other bacterial species with different morphological features and growth laws. In this context, it is pertinent to ask whether super-exponential growth is prevalent in other bacterial organisms, and not just limited to Gram-negative *E. coli* and *C. crescentus* cells. Analysis

of single-cell growth data of gram-positive *Bacillus subtilis* cells [38] reveals a non-monotonic trend in growth rate during the course of the cell cycle (Supplementary Fig 6A-B), as recently reported [31]. In particular, *B. subtilis* cells show a period of sub-exponential growth followed by a period of super-exponential growth, irrespective of growth conditions. Our model is capable of capturing these behaviors with a time-dependent λ in Eq. (2), where λ increases during the first phase of sub-exponential growth and decreases during the second phase of super-exponential growth (Supplementary Fig 6C). These observations raise questions on how time-dependent changes in growth parameters are connected to cell cycle-dependent changes in cell envelope growth pattern and protein synthesis, for which experimental data are currently lacking. A better understanding of how cellular growth parameters fluctuate during the course of the cell cycle would allow us to further refine our model assumptions and test theoretical predictions.

The biochemical model based on ribosome synthesis and resource allocation could be more finely tuned based on further experimental developments on measuring time-dependent bacterial proteome and ribosome synthesis during the cell cycle. While the production of ribosomes, cell division proteins and cell envelope proteins are accounted for in our simplified model, we neglect many metabolic proteins, transporters, and those that fall into the housekeeping/maintenance sector of the proteome. Future work taking into account these details could provide insights into the biochemical processes that are difficult to measure directly in experiments. The amount of ribosomes unused for growth, R^{U}, which is required to maintain super-exponential growth, is an interesting prediction of our model that can be tested in future experiments. Non-zero R^{U} could potentially result from ribosome degradation during the cell cycle [39] or ribosome allocation towards a proteome reserve [40], although the exact dynamics of these processes during cell cycle are not yet known. Our model also predicts that, in nutrient-rich growth environments, cells allocate proportionally more of their ribosomes to producing more ribosomes and length material rather than surface area maintenance and division proteins, suggesting that surface area and division proteins belong to the metabolic sector of the proteome [33, 34]. While these predictions are derived during steady-state growth conditions, future work predicting intra-generational dynamics of cellular resource allocation, particularly in changing nutrient conditions, would be of particular interest to the growing field of single-cell physiology.

ACKNOWLEDGEMENTS

We gratefully acknowledge support from the National Institutes of Health (NIH R35 GM143042) and the Shurl and Kay Curci Foundation. We thank Suckjoon Jun Lab (UCSD) for providing single-cell growth and shape data for *E. coli* and *B. subtilis* cells, Aaron Dinner and Norbert Scherer (University of Chicago) for providing data for *C. crescentus* cells.

METHODS

Growth rate calculation. The *E. coli* strain for the data considered from [1] is K12 NCM3722 (not-motile derivative SJ202). The K-12 MC4100 strain is used for the filamentous *E. coli* cells [6]. All growth rate data analyzed in this paper is calculated from cited timeseries length data. We perform this calculation using a midpoint derivative approximation. While this calculation loses the first and last data points, it is less noisy than a left/right approximation. We have considered a running exponential fit ($\sim$3 points) to extract κ but this method is also more noisy than the midpoint approximation. For population average data, as shown Fig. 1, we average in normalized time. The growth rate is approximated at the individual cell level and then each data point is placed into population bins according to where the data point falls in t/τ (the cell cycle time τ is specific to each cell cycle considered). We choose the number of bins in each case to be less than the average number of data points collected per cell cycle to avoid misrepresentation. Averages and error bars presented are then calculated for each bin with data from all cells. When considering individual generations rather than averages (section III onward), fits of (3) are performed on directly the length data rather considering the processed growth rates.

When obtaining values of k and λ through fitting Eq. (3) to individual cell cycles, in addition to removing outliers with non-physical parameters, we neglect the fits that result in $\lambda < 0$. These results only occur in fast growth conditions such as TSB and MOPS, accounting for less that 5% of the total cell generations. While the interpretation of $\lambda < 0$ is non-physical in the model where λ is interpreted as the length of the non-growing region of the cell envelope (Eq. 2), $\lambda < 0$ is physically permissible in the context of the ribosome model (Eq. 7), implying sub-exponential growth. Since sub-exponential growth is not observed in experimental data, the negative negative values of λ result from fitting errors for data with high intra-generational noise.

Distribution of model parameters. Constructing an analytical form for the joint probability distribution of growth parameters λ and k is challenging due to the skew in the distribution. To circumvent this difficulty, a commonly used approach is to transform the data to first remove the skew in the distribution. Given the log-normal nature of k distribution, $\ln k$ removes most of the skew from k while reflecting λ (around a chosen reference value λ_0) followed by a square root is sufficient to remove the skew. Most functions commonly used to reduce skewness are defined only on a positive domain and are also more effective if used on distributions that start without a large offset from 0, which means we must be careful about the point around which we reflect λ. For a single dataset, an easy choice is to perform a reflection such that the maximum value becomes the minimum and vice versa. However, since we aim to fit this distribution as a function of k, choosing to reflect in this manner introduces a new parameter λ_0 that can be fit from the data. It is worth noting that λ_0 only affects the efficacy with which the data are normalized rather than a modification to the data themselves. We thus define the trans-

formed variables $K = \ln k$ and $\Lambda = \sqrt{\lambda_0 - \lambda}$, which are normally distributed, allowing us to construct the joint distribution

$$P(K,\Lambda) = \frac{1}{2\pi\sigma_K\sigma_\Lambda\sqrt{1-\rho^2}} \exp\left[-\frac{1}{2(1-\rho^2)}\left[\left[\frac{K-\langle K\rangle}{\sigma_K}\right]^2 + \left[\frac{\Lambda-\langle\Lambda\rangle}{\sigma_\Lambda}\right]^2 - 2\rho\frac{(K-\langle K\rangle)(\Lambda-\langle\Lambda\rangle)}{\sigma_K\sigma_\Lambda}\right]\right] \tag{25}$$

where the distribution parameters vary with growth conditions paramterized by $\langle k\rangle$. As shown in Supplementary Fig 3, fitting appropriate mathematical functions for $\langle K\rangle$, $\langle\Lambda\rangle$, σ_k, σ_Λ, λ_0, and the correlation function $\rho(K,\Lambda)$, permits us to construct a correlated multivariate normal distribution for a given growth condition, determined by the parameter $\langle k\rangle$. Representative contour plots of the joint distribution P are shown in Fig. 2E for three different growth conditions.

It is possible to expand this framework to include the slight positive correlation between λ and L_0, as given in Table I. Considering a joint distribution including L_0 in addition to K and Λ, we have

$$P(K,\Lambda,L_0) = \frac{1}{\sqrt{2\pi\det\Sigma}} \exp\left[-\sum_{x,y}^{K,\Lambda,L_0}\frac{(x-\langle x\rangle)\Sigma_{xy}(y-\langle y\rangle)}{2}\right] \tag{26}$$

where Σ denotes the covariance matrix. In the context of determining K and Λ for a new cell, (26) takes the fixed argument of the cell's L_0 determined by the division mechanism.

For parameters defining the ribosome synthesis model, their dependencies on mean elongation rates are given by: $\sigma_k^2 = (11.14\ \text{min}^2)\langle k\rangle^4 + (2.67\cdot 10^{-5})\ \text{min}^{-2}$, $\langle\alpha'\rangle = 0.537\langle k\rangle - 0.001\ \text{min}^{-1}$, $\sigma_{\alpha'} = 0.120\langle k\rangle - 0.001\ \text{min}^{-1}$, $\langle\gamma'\rangle = 0.027\ \text{min}^{-1}$, $\sigma_{\gamma'} = 0.008\ \text{min}^{-1}$, $\langle\beta'\rangle = 0.222\langle k\rangle + 0.023\ \text{min}^{-1}$, $\sigma_{\beta'} = 0.022\ \text{min}^{-1}$.

Langevin model simulations. We briefly summarize the components that make up the Langevin model simulations. As an input, a function for mean elongation rate $\langle k(t)\rangle$ is necessary. This fixes all distributions, as seen in Figs. 2, 3, S1-S4. For each generation, growth parameters k and λ are chosen according to our correlated joint distribution (26) in addition to a value of w_0. We then integrate the stochastic differential equations (19) and (22) until division occurs, as prescribed by the adder model and a chosen Δ from fitted distribution to experimental data. We use a straightforward Euler-Maruyama method for the integration [41] using Itô calculus, neglecting the integration discretization intricacies that arise in the derivations of equations with non-constant diffusion. In each equation, the noise terms can be written as $\eta(t) = \sigma\xi(t)$, where $O(\xi) = 1/\sqrt{dt}$. To perform the integration, we take $\xi(t) = dW(t)/dt$ where dW is a zero-mean Gaussian with variance dt at each timestep (Weiner process). The noise amplitudes are determined by minimizing the difference between experimental and simulated width and length fluctuations, $\sigma_{\delta w}$ ($\approx 0.017\ \mu m$) and σ_L, respectively ($\approx 0.066\ \mu m$). We find that $\sigma_{\eta_w} \approx (0.0478\ \text{min}^{1/2}))\langle k\rangle + (0.0018\ \text{min}^{-1/2})$ and $\sigma_{\nu_k} \approx (-0.104\ \text{min}^{1/2})\langle k\rangle + (0.026\ \text{min}^{-1/2})$. During cell division, length is split according to a Gaussian division ratio r and a new w_0 for the daughter cell is chosen correlated to the old w_0 according to (15). New values of k and λ are chosen uncorrelated to the previous generation and the cell cycle repeats. A sample output of the simulation is shown in Fig. 4 depicting results for slow and fast growing media.

[1] S. Taheri-Araghi, S. D. Brown, J. T. Sauls, D. B. McIntosh, and S. Jun, Single-cell physiology, Annual Review of Biophysics **44**, 123 (2015).

[2] P. Wang, L. Robert, J. Pelletier, W. L. Dang, F. Taddei, A. Wright, and S. Jun, Robust growth of escherichia coli, Current Biology **20**, 1099 (2010).

[3] Y. Lin, S. Crosson, and N. F. Scherer, Single-gene tuning of caulobacter cell cycle period and noise, swarming motility, and surface adhesion, Molecular Systems Biology **6**, 445 (2010).

[4] S. Taheri-Araghi, S. Bradde, J. T. Sauls, N. S. Hill, P. A. Levin, J. Paulsson, M. Vergassola, and S. Jun, Cell-size control and homeostasis in bacteria, Current Biology **25**, 385 (2015).

[5] C. S. Wright, S. Banerjee, S. Iyer-Biswas, S. Crosson, A. R. Dinner, and N. F. Scherer, Intergenerational continuity of cell shape dynamics in caulobacter crescentus, Scientific Reports **5**, 1 (2015).

[6] Y. Tanouchi, A. Pai, H. Park, S. Huang, N. E. Buchler, and L. You, Long-term growth data of escherichia coli at a single-cell level, Scientific Data **4**, 1 (2017).

[7] L. Susman, M. Kohram, H. Vashistha, J. T. Nechleba, H. Salman, and N. Brenner, Individuality and slow dynamics in bacterial growth homeostasis, Proceedings of the National Academy of Sciences **115**, E5679 (2018).

[8] A. Amir, Cell size regulation in bacteria, Physical Review Letters **112**, 208102 (2014).

[9] M. Campos, I. V. Surovtsev, S. Kato, A. Paintdakhi, B. Beltran, S. E. Ebmeier, and C. Jacobs-Wagner, A constant size extension drives bacterial cell size homeostasis, Cell **159**, 1433 (2014).

[10] S. Jun and S. Taheri-Araghi, Cell-size maintenance: universal strategy revealed, Trends in Microbiology **23**, 4 (2015).

[11] S. Banerjee, K. Lo, M. K. Daddysman, A. Selewa, T. Kuntz, A. R. Dinner, and N. F. Scherer, Biphasic growth dynamics control cell division in caulobacter crescentus, Nature microbiology **2**, 1 (2017).

[12] S. Jun, F. Si, R. Pugatch, and M. Scott, Fundamental principles in bacterial physiology—history, recent progress, and the future with focus on cell size control: a review, Reports on Progress in Physics **81**, 056601 (2018).

[13] F. Si, G. Le Treut, J. T. Sauls, S. Vadia, P. A. Levin, and S. Jun, Mechanistic origin of cell-size control and homeostasis in bacteria, Current Biology **29**, 1760 (2019).

[14] F. Si, D. Li, S. E. Cox, J. T. Sauls, O. Azizi, C. Sou, A. B. Schwartz, M. J. Erickstad, Y. Jun, X. Li, *et al.*, Invariance of initiation mass and predictability of cell size in escherichia coli,

Current Biology **27**, 1278 (2017).

[15] H. Zheng, Y. Bai, M. Jiang, T. A. Tokuyasu, X. Huang, F. Zhong, Y. Wu, X. Fu, N. Kleckner, T. Hwa, *et al.*, General quantitative relations linking cell growth and the cell cycle in escherichia coli, Nature Microbiology **5**, 995 (2020).

[16] D. Serbanescu, N. Ojkic, and S. Banerjee, Cellular resource allocation strategies for cell size and shape control in bacteria, The FEBS Journal (2021).

[17] L. K. Harris and J. A. Theriot, Relative rates of surface and volume synthesis set bacterial cell size, Cell **165**, 1479 (2016).

[18] E. R. Oldewurtel, Y. Kitahara, and S. van Teeffelen, Robust surface-to-mass coupling and turgor-dependent cell width determine bacterial dry-mass density, Proceedings of the National Academy of Sciences **118**, 10.1073/pnas.2021416118 (2021).

[19] N. Ojkic, D. Serbanescu, and S. Banerjee, Surface-to-volume scaling and aspect ratio preservation in rod-shaped bacteria, eLife **8** (2019).

[20] S. Banerjee, K. Lo, N. Ojkic, R. Stephens, N. F. Scherer, and A. R. Dinner, Mechanical feedback promotes bacterial adaptation to antibiotics, Nature Physics **17**, 403 (2021).

[21] J. Nguyen, V. Fernandez, S. Pontrelli, U. Sauer, M. Ackermann, and R. Stocker, A distinct growth physiology enhances bacterial growth under rapid nutrient fluctuations, Nature Communications **12**, 1 (2021).

[22] M. Panlilio, J. Grilli, G. Tallarico, I. Iuliani, B. Sclavi, P. Cicuta, and M. C. Lagomarsino, Threshold accumulation of a constitutive protein explains e. coli cell-division behavior in nutrient upshifts, Proceedings of the National Academy of Sciences **118** (2021).

[23] S. Bakshi, E. Leoncini, C. Baker, S. J. Cañas-Duarte, B. Okumus, and J. Paulsson, Tracking bacterial lineages in complex and dynamic environments with applications for growth control and persistence, Nature Microbiology **6**, 783 (2021).

[24] S. Iyer-Biswas, C. S. Wright, J. T. Henry, K. Lo, S. Burov, Y. Lin, G. E. Crooks, S. Crosson, A. R. Dinner, and N. F. Scherer, Scaling laws governing stochastic growth and division of single bacterial cells, Proceedings of the National Academy of Sciences **111**, 15912 (2014).

[25] Y. Chen, R. Baños, and J. Buceta, A markovian approach towards bacterial size control and homeostasis in anomalous growth processes, Scientific Reports **8** (2018).

[26] A. S. Sassi, M. Garcia-Alcala, P. Cluzel, and Y. Tu, Multiplicative noise underlies taylor's law in protein concentration fluctuations in single cells (2021).

[27] O. M. Romano and M. Cosentino Lagomarsino, Single rod-shaped cell fluctuations from stochastic surface and volume growth rates, Phys. Rev. E **101**, 042403 (2020).

[28] S. Banerjee, N. F. Scherer, and A. R. Dinner, Shape dynamics of growing cell walls, Soft Matter **12**, 3442 (2016).

[29] M. Godin, F. F. Delgado, S. Son, W. H. Grover, A. K. Bryan, A. Tzur, P. Jorgensen, K. Payer, A. D. Grossman, M. W. Kirschner, *et al.*, Using buoyant mass to measure the growth of single cells, Nature methods **7**, 387 (2010).

[30] P. Kar, S. Tiruvadi-Krishnan, J. Männik, J. Männik, and A. Amir, Distinguishing different modes of growth using single-cell data, eLife **10**, e72565 (2021).

[31] N. Nordholt, J. H. van Heerden, and F. J. Bruggeman, Biphasic cell-size and growth-rate homeostasis by single bacillus subtilis cells, Current Biology **30**, 2238 (2020).

[32] Y.-J. Sun, F. Bai, A.-C. Luo, X.-Y. Zhuang, T.-S. Lin, Y.-C. Sung, Y.-L. Shih, and C.-J. Lo, Probing bacterial cell wall growth by tracing wall-anchored protein complexes, Nature Communications **12**, 2160 (2021).

[33] M. Scott, C. W. Gunderson, E. M. Mateescu, Z. Zhang, and T. Hwa, Interdependence of cell growth and gene expression: origins and consequences, Science **330**, 1099 (2010).

[34] D. Serbanescu, N. Ojkic, and S. Banerjee, Nutrient-dependent trade-offs between ribosomes and division protein synthesis control bacterial cell size and growth, Cell reports **32**, 108183 (2020).

[35] F. Bertaux, J. Von Kügelgen, S. Marguerat, and V. Shahrezaei, A bacterial size law revealed by a coarse-grained model of cell physiology, PLoS Computational Biology **16**, e1008245 (2020).

[36] M. Schaechter, O. Maaløe, and N. O. Kjeldgaard, Dependency on medium and temperature of cell size and chemical composition during balanced growth of salmonella typhimurium, Microbiology **19**, 592 (1958).

[37] C. W. Gardiner, *Handbook of Stochastic Methods for Physics, Chemistry and the Natural Sciences* (Springer, 2004).

[38] J. T. Sauls, S. E. Cox, Q. Do, V. Castillo, Z. Ghulam-Jelani, and S. Jun, Control of bacillus subtilis replication initiation during physiological transitions and perturbations, mBio **10**, e02205 (2019).

[39] L. Calabrese, J. Grilli, M. Osella, C. P. Kempes, M. C. Lagomarsino, and L. Ciandrini, Protein degradation sets the fraction of active ribosomes at vanishing growth, PLOS Computational Biology **18**, e1010059 (2022).

[40] M. Mori, S. Schink, D. W. Erickson, U. Gerland, and T. Hwa, Quantifying the benefit of a proteome reserve in fluctuating environments, Nature Communications **8**, 1 (2017).

[41] E. P. Peter E. Kloeden, *Numerical Solution of Stochastic Differential Equations* (Springer, 1992).